Atom-Based Vector Microwave Electrometry Using Rubidium Rydberg Atoms in a Vapor Cell

J. A. Sedlacek,[1] A. Schwettmann,[1] H. Kübler,[1,2] and J. P. Shaffer[1,*]

[1]*Homer L. Dodge Department of Physics and Astronomy, The University of Oklahoma, 440 West Brooks Street, Norman, Oklahoma 73019, USA*

[2]*5. Physikalisches Institut, Universität Stuttgart, Pfaffenwaldring 57 D-70550 Stuttgart, Germany*

(Received 15 April 2013; published 6 August 2013)

It is clearly important to pursue atomic standards for quantities like electromagnetic fields, time, length, and gravity. We have recently shown using Rydberg states that Rb atoms in a vapor cell can serve as a practical, compact standard for microwave electric field strength. Here we demonstrate for the first time that Rb atoms excited in a vapor cell can also be used for vector microwave electrometry by using Rydberg-atom electromagnetically induced transparency. We describe the measurements necessary to obtain an arbitrary microwave electric field polarization at a resolution of 0.5°. We compare the experiments to theory and find them to be in excellent agreement.

DOI: 10.1103/PhysRevLett.111.063001 PACS numbers: 32.80.Rm, 03.50.De, 07.50.Ls, 42.62.Fi

Quantum systems, such as atoms, have already been adopted as time and length standards because they offer significant advantages for making stable and uniform measurements of these quantities [1,2]. Atoms have also been successfully used for magnetometry, reaching impressive sensitivity and spatial resolutions [3–8]. Despite these successes, it is only recently that atoms have been used for practical microwave (MW) electrometry and achieved sensitivities below current standards by exploiting the properties of Rydberg atoms [9]. Rydberg atoms have been used for electrometry for some time but almost exclusively in elaborate laboratory setups [10–21].

The relative lag of atom-based electrometry compared to magnetometry is not simply due to a lack of importance. The accurate measurement of MW electric field strength and polarization offers interesting possibilities for antenna calibration and MW electronics development, as well as for realizing an atomic candle for MW electric field stabilization [22,23], to name a few important examples. Atom-based MW electrometry, therefore, has the potential to lead to revolutionary advances in the development of MW electronics, advanced radar applications, and materials used in MW systems. So far, only the magnetic field has been accessible in the near-field MW regime [24,25], and our method can be valuable for measuring MW electric fields in the near field. Recall, there is not generally a straightforward relation between the MW magnetic and electric fields in the near field.

In this Letter, we demonstrate a scheme for vector MW electrometry using Rydberg-atom electromagnetically induced transparency (EIT) [26,27] in Rb atomic vapor cells. We achieve an angular resolution of 0.5° and show the method can be realized by comparing experimental data to theory. The vector measurements here are compatible with our prior work where we attained a minimum detectable electric field amplitude of $\sim 8\ \mu\mathrm{V\,cm^{-1}}$ and a sensitivity of $\sim 30\ \mu\mathrm{V\,cm^{-1}\,Hz^{-1/2}}$ [9]. To date, EIT has been principally used for vector magnetometry [28,29].

To measure the strength and polarization of a MW electric field, we use the Rb level system shown in Fig. 1(a). In the three-level system, $5S_{1/2}$-$5P_{3/2}$-$53D_{5/2}$, quantum interference can create a "dark state" that prohibits resonant absorption of a probe laser, Fig. 1(b) (black). Coupling a fourth level to this Rydberg-atom EIT system, $54P_{3/2}$, with a MW electric field can create a "bright state" that causes probe photons to again be absorbed on resonance [9,30–33]. The bright state induced by the MW electric field can manifest itself in the probe absorption spectrum as a splitting of the dark state for large enough MW electric field amplitudes, Fig. 1(b) (red). In contrast to sensing only MW electric field strength, we present a significant extension of our method where, for the first time, we show it is capable of measuring the vector character, or polarization, of the MW electric field.

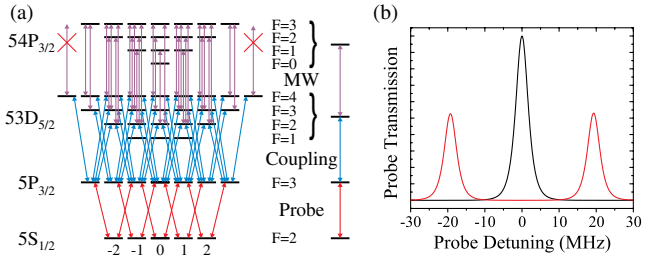

FIG. 1 (color online). (a) Level diagram showing all 52 possible states addressed by the experiment. The arrows indicate allowed excitations for the σ-polarized probe and coupling beams and π-polarized MWs. The $54P_{3/2}$ states are shown above the $53D_{5/2}$ states for simplicity. On the right, the corresponding effective four-level system is shown. (b) Theoretical line shapes resulting from a three-level (black) and four-level (red) system.

EIT is known to be sensitive to the laser polarizations [34–36]. The MW electric field polarization can be determined from the probe laser transmission by recognizing that the $53D_{5/2}$ ($F = 4$, $m_F = \pm 4$) states can be coupled to, or uncoupled from, the $54P_{3/2}$ manifold depending on the probe and coupling laser polarization relative to that of the MW electric field. Some excitation pathways present in the system shown in Fig. 1(a) that pass through the stretched $53D_{5/2}$ ($F = 4$, $m_F = \pm 4$) states are restricted to the three levels of the EIT ladder system, $5S_{1/2}$-$5P_{3/2}$-$53D_{5/2}$. Other excitation pathways take the system through the nonstretched $53D_{5/2}$ states and can experience the full four-level system. The behavior of the entire 52-state system can be understood by considering a few cases of laser and MW electric field polarizations. Figure 2 shows key polarization combinations that illustrate the behavior for selected laser and MW electric field polarizations. Experimental data and theoretical results obtained from a density matrix approach to the 52-state system, including Doppler averaging [9], are shown.

The case where the probe and coupling lasers are linearly polarized along the same direction as the MWs, $\xi = 0°$ and $\zeta = 90°$, where ξ and ζ are defined in Fig. 3 is shown in Fig. 2 (black). In this case, π transitions are driven throughout the system and all the excitation pathways experience a four-level system. The theoretical and experimental spectra have two transmission peaks separated by $(\lambda_c/\lambda_p)\Omega_{\mathrm{MW}}$, where λ_p is the probe, λ_c the coupling laser wavelength, and Ω_{MW} is the MW Rabi frequency [9]. The probe laser is absorbed on resonance.

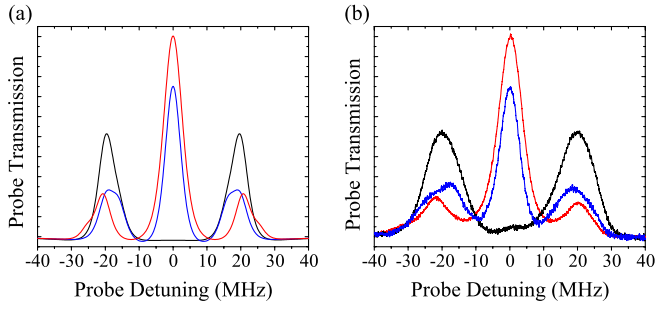

FIG. 2 (color online). Theoretical (a) and experimental (b) results for the illustrative polarization cases described in the text: probe laser, coupling laser, and MWs $\hat{x}$ polarized (black); probe and coupling laser $\hat{y}$ polarized and MWs $\hat{x}$ polarized (blue); probe and coupling lasers σ^+ polarized and MWs $\hat{z}$ polarized (red). The additional line broadening observed in the experiment is due to the MWs being inhomogeneous over the extent of the vapor cell. The effect resulted from the positioning of the antenna that was required to avoid unwanted reflections in our laboratory. The slight asymmetry in the data is due to a small amount of ionization. This effect did not significantly affect our measurements but can be reduced by driving the Rydberg transition with higher Rabi frequency. Our experiment is limited by the amount of blue laser power available.

Also displayed in Fig. 2 (red) is the case where the probe and coupling lasers are σ^+ polarized and excite $\Delta m_F = +1$ transitions. The atoms are optically pumped such that the stretched states of the $5S_{1/2}$, $5P_{3/2}$, and $54D_{5/2}$ manifolds dominate. The MW electric field is polarized in the $\hat{z}$ direction. In this case, the three-level excitation pathways are overwhelmingly favored since a π MW transition cannot couple the stretched states to the $54P_{3/2}$ manifold. The experimental results shown support this explanation as a large probe transmission peak is observed on resonance.

If the probe and coupling lasers are both linearly polarized parallel to each other, e.g., $\hat{y}$ polarized, but orthogonal to the MW electric field polarization, e.g., $\hat{z}$ polarized, there are both three-level and four-level excitation pathways open, Fig. 2 (blue). This behavior derives from the fact that in a $\hat{z}$-atomic basis the MW electric field drives π transitions, while the $\hat{y}$-polarized probe and coupling lasers drive transitions throughout the $53D_{5/2}$ manifold, as they are in a superposition of σ^+ and σ^- polarizations in the $\hat{z}$ basis. The experimental and theoretical spectra show reduced probe transmission on resonance and two probe transmission peaks split by $(\lambda_c/\lambda_p)\Omega_{\mathrm{MW}}$.

Any MW electric field can be split into a component that couples atoms to the $54P_{3/2}$ state and one that does not. The relative strength of the components only depends on the MW electric field polarization relative to the polarization and propagation direction of the two laser beams. When rotating parallel linear probe and coupling laser polarizations around their propagation axes, the projection of the MW electric field on the probe and coupling laser polarization changes. The change of the MW electric field polarization projection relative to the laser polarizations results in a variation of the probe laser transmission. The probe laser transmission changes can be used to determine the MW electric field polarization since the probe and coupling laser polarizations are known. The splitting of the peaks indicative of the four-level behavior remains relatively constant because this is largely determined by the electric field amplitude that the atoms experience and can be used to find the amplitude of the MW electric field in conjunction with the polarization measurement.

The geometry needed to describe a measurement of the MW electric field polarization is shown in Fig. 3. The incident MW electric field vector $\vec{E}$ forms an angle ζ_z with the space fixed propagation direction of the probe laser chosen to lie along the $\hat{z}$ axis. E_z is the projection of the MW electric field on $\hat{z}$. The perpendicular component of the MW electric field $\vec{E}_{\perp z}$ forms an angle ξ_z with the polarization vector of the probe and coupling laser beams in the $\hat{x}$-$\hat{y}$ plane. The angle φ_z between the $\hat{x}$ axis and $\vec{E}_{\perp z}$ can be determined by rotating the probe and coupling laser polarizations. In this case, the configuration is periodically changing from the case where $\vec{E}_{\perp z}$ and the laser fields are parallel, Fig. 2 (black), to the case where the MW and laser

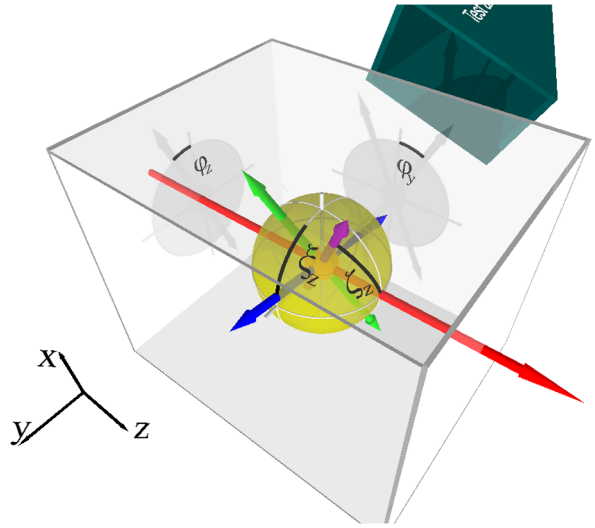

FIG. 3 (color online). Schematic view of the setup including the cell in the foreground and the test antenna in the background. The laser propagation direction (red), the polarization of the two laser beams (blue), and an arbitrary polarization direction of the MW (magenta) are shown together with the relevant angles between them as described in the main text. The shadows are the projections onto the $\hat{x}$-$\hat{y}$ plane on the left and the $\hat{x}$-$\hat{z}$ plane in the back.

fields are orthogonal, Fig. 2 (blue). For simultaneous rotation of the probe and coupling laser beam polarizations about $\hat{z}$, ξ_z, Fig. 3; the probe transmission on resonance will oscillate between a minimum for $\xi_z = 0°$, Fig. 2 (black), and a maximum for $\xi_z = 90°$, Fig. 2 (blue). The amplitude of this oscillation measures ζ_z, the projection angle along $\hat{z}$, since with increasing ζ_z, $\vec{E}_{\perp z}$ increases. Measuring φ and ζ along all three Cartesian coordinate axes reveals the following:

$$\varphi_z = \tan^{-1}\left(\frac{E_x}{E_y}\right), \qquad \zeta_z = \tan^{-1}\left(\frac{|E_{\perp z}|}{|E_z|}\right), \tag{1a}$$

$$\varphi_x = \tan^{-1}\left(\frac{E_y}{E_z}\right), \qquad \zeta_x = \tan^{-1}\left(\frac{|E_{\perp x}|}{|E_x|}\right), \tag{1b}$$

$$\varphi_y = \tan^{-1}\left(\frac{E_x}{E_z}\right), \qquad \zeta_y = \tan^{-1}\left(\frac{|E_{\perp y}|}{|E_y|}\right). \tag{1c}$$

The information obtained from measuring the three angles φ_i is sufficient to determine the MW electric field polarization. The magnitude of the MW electric field can be obtained from the splitting of the transmission peaks observed as a consequence of the four-level behavior. It is important to note that it is impossible to distinguish the angle ζ_i from $180° - \zeta_i$ (magenta and green arrow in Fig. 3 for $i = z$) because these two cases differ only in the relative phase between E_i and $E_{\perp i}$.

A simplified model of the resonant probe transmission dependence on ξ_i can be obtained by considering the projection of $\vec{E}$ onto the probe and coupling laser polarization. From Fig. 3 the projection of $\vec{E}$ on the laser polarization direction is $E_\parallel = |\vec{E}|\cos(\xi)\sin(\zeta)$. Because of branching between the three- and four-level behavior, the resonant probe transmission can be approximated as $T = 1 - (E_\parallel/|\vec{E}|)^2 = 1 - \cos^2(\xi)\sin^2(\zeta)$. The approximation does not reproduce the probe transmission amplitude very well. However, the positions of the minima and maxima as ξ_i is varied are predicted accurately.

The experimental setup Fig. 3 consists of a probe laser beam and a coupling laser beam that are overlapped and counterpropagate through a cuboidal atomic Rb cell with dimensions (10 mm × 10 mm × 30 mm). The probe laser is an extended cavity diode laser (ECDL) at ~780 nm that propagates along the $\hat{z}$ axis. The coupling laser is derived from a homebuilt frequency doubling system operating at ~480 nm and propagates along $-\hat{z}$. The doubled light is generated from an amplified ECDL at 960 nm. The probe laser is locked to the ^{87}Rb $5S_{1/2}(F = 2) \rightarrow 5P_{3/2}(F = 1, 3)$ crossover peak. The 960 nm ECDL is locked to a Fabry-Perot cavity that is stabilized to an EIT signal generated in a separate vapor cell. The laser linewidths are ~700 kHz. An acousto-optic modulator is used to scan the probe laser frequency around the $5S_{1/2}(F = 2) \rightarrow 5P_{3/2}(F = 3)$ transition. An intensity stabilization circuit based on a field programmable gate array [37] is used to intensity stabilize the probe laser to ~0.1%. The polarizations of the laser beams are adjusted and filtered using wave plates and Glan laser polarizers. The probe (coupling) laser spot size is 200(65) μm and the power is 15 μW (11 mW). The corresponding probe (coupling) Rabi frequency is $2\pi \times 8.1(2\pi \times 3.4)$ MHz.

MWs are generated at 14.233 GHz with a signal generator. The MWs are coupled into a horn antenna that illuminates the Rb vapor cell, Fig. 3. The polarization of the MWs is linear, and it is changed in the experiment by rotating the antenna. The transition dipole moment for the transition between the Rydberg states is calculated to be 4103 D [38]. The MW intensity used for the experiments was 1.27×10^{-3} mW cm^{-2}. This corresponds to a Rabi frequency of $2\pi \times 64$ MHz. For these parameters, the 52-state theory yields a probe transmission peak splitting of 39.36 MHz. The probe transmission peak splitting observed in the experiment is 39.36 ± 0.06 MHz, Fig. 2(b) (black).

The intensity of the coupling laser is modulated at 40 kHz, and the probe transmission is detected on a photodiode. The photodiode signal is processed using a lock-in amplifier. The experimental data are a result of 20 averages. Three pairs of orthogonal Helmholtz coils surround the cell to cancel the background geomagnetic field to a level of <0.1 G. The experiment is conducted at a Rb vapor cell temperature of 45 °C. The temperature corresponds to a Rb vapor pressure of 2.6×10^{-6} Torr. The cell was heated to prevent significant condensation of Rb on the walls of the vapor cell. Condensation of Rb on the walls of the vapor cell causes reflections of the MWs.

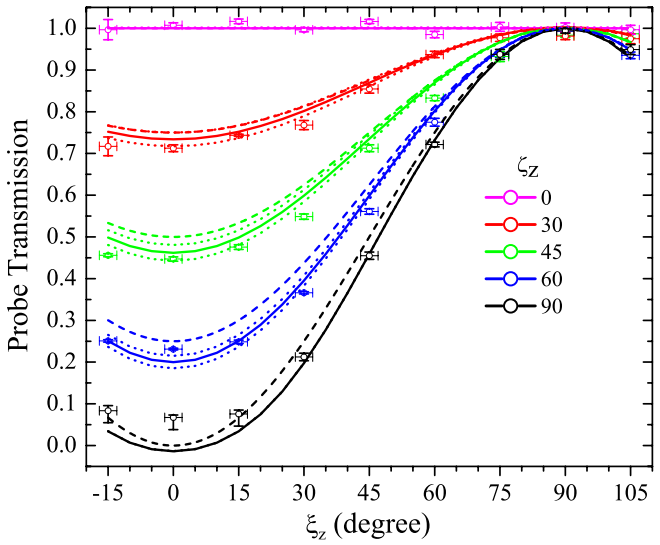

FIG. 4 (color online). Probe laser transmission on resonance for different angles between the laser polarizations and the MW electric field vector. The vertical error bars for the experimental points are due to statistical errors in the measured peak height while the horizontal error bars are due to systematic uncertainty in ξ. Fifty-two-state theoretical results (solid lines) with $\pm 1°$ uncertainty in ζ (dotted lines). The curves for $1 - (E_{\|}/|\vec{E}|)^2 = 1 - \cos^2(\xi)\sin^2(\zeta)$ are also shown (dashed lines). The probe transmission is normalized such that the maximum theoretical transmission is 1. The deviation of the points with larger ζ around $\xi = 0°$ is due to polarization impurities in the laser and MW beams. The angular resolution of $\sim 0.5°$ is derived from a least squares fit of each trace to the theory. A three-direction measurement would yield reduced resolution as three different measurements must be combined.

Figure 4 shows an example of a measurement used to determine the MW electric field polarization. The pump and probe polarizations are rotated through $\xi_z = 120°$ for different MW antenna angles, ζ_z. The transmission of the probe laser on resonance is plotted in the figure as a function of ξ_z for different ζ_z. The direction of $\vec{E}_{\perp z}$ can be found because the on-resonance probe transmission is minimum for probe and coupling laser polarizations parallel to $\vec{E}_{\perp z}$. The angle ζ_z between the MW electric field polarization and the laser propagation axis is determined by the modulation depth of the on-resonance probe transmission as a function of ξ_z. Our calculations indicate the method also works for elliptical or circularly polarized light but require measurement along more than one axis and the relative polarizations of the probe and coupling laser to change.

The maximum sensitivity is obtained when the four-level peaks are completely split from the three-level peak. For our experimental parameters this occurs at a MW electric field amplitude of $\sim 10\ \mathrm{mV\,cm^{-1}}$. Increasing the MW electric field strength has little effect on the central peak until $\sim 100\ \mathrm{mV\,cm^{-1}}$. At this point, the peak starts to shift and decrease in height, most likely due to multiphoton transitions [9]. The angular resolution detected in the experiment is $\sim 0.5°$ in both ζ and φ. Narrower laser linewidths, lower noise electronics, purer polarizations, and better laser intensity stabilization can significantly improve the sensitivity.

In summary, we have demonstrated an atom-based method for sensitively measuring the polarization of a MW electric field by making use of Rydberg states in a Rb vapor cell. The vector electrometry described here is compatible with measurements of the electric field amplitude as presented in our earlier work [9] and is therefore practical for making atom-based measurements of the MW electric field in compact portable setups for discrete Rydberg states in the range of 1–500 GHz. The Rydberg states can be tuned with magnetic and electric fields but such tuning is problematic for absolute electric field measurement to the extent the fields change the transition dipole moment [9]. We were able to achieve an angular resolution of $\sim 0.5°$ in both ζ and φ. Our approach allowed for miniaturization on the mm or even sub-mm scale [39]. Because of the optical readout and materials used, distortion of the electric field was relatively small compared to dipole antennas.

We thank T. Pfau and Robert Löw for useful discussions. This work was supported by the DARPA QuASAR program through a grant from ARO (Grant No. 60181-PH-DRP) and the NSF (Grant No. PHY-1104424).

*shaffer@nhn.ou.edu

[1] J. Hall, Rev. Mod. Phys. **78**, 1279 (2006).
[2] D. Hanneke, S. Fogwell, and G. Gabrielse, Phys. Rev. Lett. **100**, 120801 (2008).
[3] D. Budker and M. Romalis, Nat. Phys. **3**, 227 (2007).
[4] B. Patton, O. O. Versolato, D. C. Hovde, E. Corsini, J. M. Higbie, and D. Budker, Appl. Phys. Lett. **101**, 083502 (2012).
[5] I. M. Savukov, S. J. Seltzer, M. V. Romalis, and K. L. Sauer, Phys. Rev. Lett. **95**, 063004 (2005).
[6] M. V. Balabas, T. Karaulanov, M. P. Ledbetter, and D. Budker, Phys. Rev. Lett. **105**, 070801 (2010).
[7] W. Wasilewski, K. Jensen, H. Krauter, J. J. Renema, M. V. Balabas, and E. S. Polzik, Phys. Rev. Lett. **104**, 133601 (2010).
[8] M. Koschorreck, M. Napolitano, B. Dubost, and M. W. Mitchell, Phys. Rev. Lett. **104**, 093602 (2010).
[9] J. A. Sedlacek, A. Schwettmann, H. Kübler, R. Löw, T. Pfau, and J. P. Shaffer, Nat. Phys. **8**, 819 (2012).
[10] A. Osterwalder and F. Merkt, Phys. Rev. Lett. **82**, 1831 (1999).
[11] M. G. Bason, M. Tanasittikosol, A. Sargsyan, A. K. Mohapatra, D. Sarkisyan, R. M. Potvliege, and C. S. Adams, New J. Phys. **12**, 065015 (2010).
[12] R. P. Abel, C. Carr, U. Krohn, and C. S. Adams, Phys. Rev. A **84**, 023408 (2011).
[13] L. A. Jones, J. D. Carter, and J. D. D. Martin, Phys. Rev. A **87**, 023423 (2013).

[14] J. D. Carter, O. Cherry, and J. D. D. Martin, Phys. Rev. A **86**, 053401 (2012).
[15] P. P. Herrmann, J. Hoffnagle, N. Schlumpf, V. L. Telegdi, and A. Weis, J. Phys. B **19**, 1271 (1986).
[16] A. Schramm, J. M. Weber, J. Kreil, D. Klar, M.-W. Ruf, and H. Hotop, Phys. Rev. Lett. **81**, 778 (1998).
[17] A. Tauschinsky, R. M. T. Thijssen, S. Whitlock, H. B. van Linden van den Heuvell, and R. J. C. Spreeuw, Phys. Rev. A **81**, 063411 (2010).
[18] P. Goy, L. Moi, M. Gross, J. M. Raimond, C. Fabre, and S. Haroche, Phys. Rev. A **27**, 2065 (1983).
[19] M. Auzinsh, L. Jayasinghe, L. Oelke, R. Ferber, and N. Shafer-Ray, J. Phys. D **34**, 1933 (2001).
[20] M. T. Frey, X. Ling, B. G. Lindsay, K. A. Smith, and F. B. Dunning, Rev. Sci. Instrum. **64**, 3649 (1993).
[21] H. Figger, G. Leuchs, R. Straubinger, and H. Walther, Opt. Commun. **33**, 37 (1980).
[22] J. C. Camparo, Phys. Rev. Lett. **80**, 222 (1998).
[23] T. Swan-Wood, J. G. Coffer, and J. C. Camparo, IEEE Trans. Instrum. Meas. **50**, 1229 (2001).
[24] P. Böhi, M. F. Riedel, T. W. Hänsch, and P. Treutlein, Appl. Phys. Lett. **97**, 051101 (2010).
[25] P. Böhi and P. Treutlein, Appl. Phys. Lett. **101**, 181107 (2012).
[26] M. Fleischhauer, A. Imamoglu, and J. P. Marangos, Rev. Mod. Phys. **77**, 633 (2005).
[27] A. K. Mohapatra, T. R. Jackson, and C. S. Adams, Phys. Rev. Lett. **98**, 113003 (2007).
[28] K. Cox, V. I. Yudin, A. V. Taichenachev, I. Novikova, and E. E. Mikhailov, Phys. Rev. A **83**, 015801 (2011).
[29] V. I. Yudin, A. V. Taichenachev, Y. O. Dudin, V. L. Velichansky, A. S. Zibrov, and S. A. Zibrov, Phys. Rev. A **82**, 033807 (2010).
[30] B. K. Dutta and P. K. Mahapatra, Phys. Scr. **75**, 345 (2007).
[31] H. Schmidt and A. Imamoglu, Opt. Lett. **21**, 1936 (1996).
[32] M. D. Lukin, S. F. Yelin, M. Fleischhauer, and M. O. Scully, Phys. Rev. A **60**, 3225 (1999).
[33] S. N. Sandhya and K. K. Sharma, Phys. Rev. A **55**, 2155 (1997).
[34] D. McGloin, M. H. Dunn, and D. J. Fulton, Phys. Rev. A **62**, 053802 (2000).
[35] Y.-C. Chen, C.-W. Lin, and I. A. Yu, Phys. Rev. A **61**, 053805 (2000).
[36] Y.-W. Chen, C.-W. Lin, Y.-C. Chen, and I. A. Yu, J. Opt. Soc. Am. B **19**, 1917 (2002).
[37] A. Schwettmann, J. Sedlacek, and J. P. Shaffer, Rev. Sci. Instrum. **82**, 103103 (2011).
[38] M. J. Piotrowicz, C. MacCormick, A. Kowalczyk, S. Bergamini, I. I. Beterov, and E. A. Yakshina, New J. Phys. **13**, 093012 (2011).
[39] H. Kübler, J. P. Shaffer, T. Baluktsian, R. Löw, and T. Pfau, Nat. Photonics **4**, 112 (2010).